Comprehensive Comparison of Modular Multilevel Converter Internal Energy Balancing Methods

Stefan Milovanović, *Student Member, IEEE*, and Dražen Dujić, *Senior Member, IEEE*

***Abstract*—Stacking of floating structures, known as submodules or cells, provides the modular multilevel converter with theoretically unlimited voltage scalability. However, such a convenience comes at a price of increased control complexity, especially in the domain of internal energy control. In other words, energies of the submodule clusters must be controlled to their setpoint values; otherwise, stable and high-performance operation of the converter cannot be ensured. So far, several approaches toward balancing of the modular multilevel converter internal energy, in both vertical and horizontal directions, have been proposed. Nevertheless, differences among them have never been analytically supported. In this article, three seemingly different energy balancing strategies are thoroughly explained, providing a framework for the theoretical comparison of different dynamic responses provided by them. All the results are verified on the large-scale hardware-in-the-loop platform, serving as a digital twin of a grid-connected 3.3-kVac/5-kVdc 1.25-MW converter being driven by the industrial ABB PEC800 controller.**

***Index Terms*—Chainlink converters, energy balancing, energy control, modular multilevel converter (MMC).**

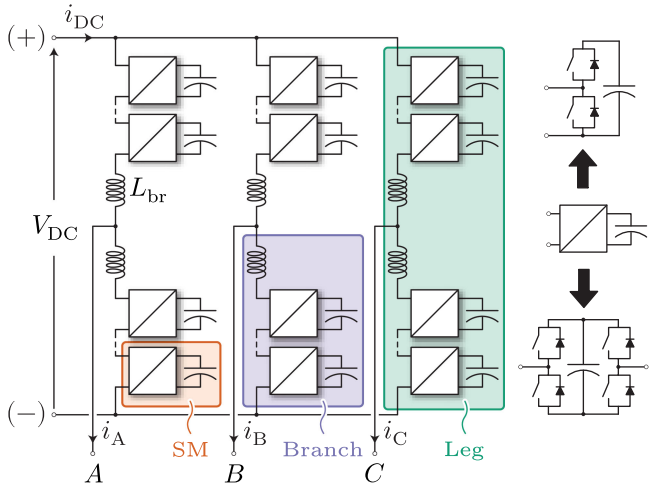

Fig. 1. MMC with the adopted naming convention.

I. Introduction

OWING to outstanding flexibility and scalability, a modular multilevel converter (MMC) [1], [2], presented in Fig. 1, has become an attractive solution for a vast variety of applications spanning both medium-voltage and high-voltage domains. The so-called submodule (SM) represents the basic building block of any chainlink converter [3], including the MMC itself. Depending on the application, SMs are mainly realized as half-bridge or full-bridge, not excluding the other options mentioned in [4] and [5]. According to Fig. 1, a cluster of SMs in series connection with an inductor L_{br} is referred to as the branch, whereas two branches comprise the leg. It is straightforward to note that the MMC employs distributed and, more importantly, floating dc links. Although the SM represents an independent single-phase conversion stage, analysis of the MMC considers every branch to be an entity characterized by its energy storage nature [6], [7]. The total energy stored within a branch provides an image of voltage across its SM capacitors; consequently, the need for the internal energy control becomes evident.

The total energy stored inside the MMC can be controlled from either dc or ac terminals, depending on the employed operating mode (inverter/rectifier). However, equal energy distribution needs to be ensured in both horizontal and vertical directions. Energy exchange among the legs, by means of the suitable circulating current components, which are going to be introduced shortly, implies the energy shift in horizontal direction, hence the name horizontal balancing. On the other hand, energy exchange between two branches belonging to the same leg is referred to as vertical balancing. Apart from ensuring equal energy distribution among the branches, the control algorithm must ensure equal distribution of energy among the SMs belonging to the same branch. This, however, strongly depends on the employed modulator structure, as discussed in [8]–[10], and this subject falls out of this article's scope. Henceforward, the term energy balancing will be used to denote the branch/leg energy shifts, while assuming uniform energy distribution among the SMs of an observed branch.

The subject of energy balancing has been addressed by various authors so far; notwithstanding, all the approaches known to the scientific community revolve around three main ideas summarized in Table I, while the term singular value decomposition (SVD) will be explained in the upcoming sections. For

Manuscript received July 31, 2020; revised September 21, 2020 and November 21, 2020; accepted January 14, 2021. Date of publication January 19, 2021; date of current version May 5, 2021. This work was supported in part by the European Union's Horizon 2020 Research and Innovation Programme under Grant 881772 (FUNDRES project) and in part by the Swiss Innovation Agency - Innosuisse, under the Innovation Project 38041.1 IP-ENG. Recommended for publication by Associate Editor D. G. Xu. *(Corresponding author: Stefan Milovanović.)*

The authors are with the Power Electronics Laboratory, École Polytechnique Fédérale de Lausanne, 1015 Lausanne, Switzerland (e-mail: stefan.milovanovic@epfl.ch; drazen.dujic@epfl.ch).

Color versions of one or more figures in this article are available at https://doi.org/10.1109/TPEL.2021.3052607.

Digital Object Identifier 10.1109/TPEL.2021.3052607

TABLE I
SHORT SUMMARY OF THE ANALYZED BALANCING METHODS

	Method 1 [11]	Method 2 [12]	Method 3 [13]
Horizontal balancing	SVD-based approach	Circ. currents ctrl. in the $\alpha\beta$- domain	Circ. currents ctrl. in the $\alpha\beta$- domain
Vertical balancing	SVD-based approach	Injection of reactive components into circ. currents	Circ. currents +/− sequence control

example, energy controllers described in [14] or [15], [16] represent an extended variation of the controller described in [13]. In [17], it was shown that different selection of circulating current optimization criteria leads to the references obtained through the use of controllers from [11] and [12]. Similarly, results already available in [11] and [12] were presented in [18]. In [19], the horizontal balancing principle identical to the one described in [11] was proposed, whereas the challenge of vertical balancing was solved, as discussed in [13].

Comparison between the approaches described in [11] and [12] can be found in [20]; however, different responses provided by the two were never analytically supported or discussed beyond the level of observations. Moreover, despite achieving the identical end goals, energy balancing proposals made in [11]–[13] follow completely different lines of thinking, and the question on what connects them has never been raised before. This article, for the first time, provides a thorough analytic connection among balancing methods from [11]–[13], and it can be considered its first contribution.

The main goal of [11] was to propose the general concept of energy balancing in an arbitrary MMC-based circuit. In other words, the SVD-based energy balancing method can be used in complex structures, such as the matrix MMC [21] or even the MMC operating with parallel branches [22], [23]. Such, rather mathematical, approach is not widely recognized in the power electronics community, and detailed explanation, along with the physical connotation, of the logic underlying it was not provided in [11]. Obviously, certain theoretical gaps still exist, and this article aims at filling them in a comprehensive manner, which is considered its second contribution.

The rest of this article is organized as follows. Section II provides a brief recapitulation of the MMC operating principles along with the definition of quantities used hereafter. A thorough discussion on the MMC internal energy balancing approaches can be found in Section III, whereas Section IV contains a comprehensive analysis enabling their straightforward comparison. Section V includes results obtained on a large-scale hardware-in-the-loop (HIL) setup serving as a digital twin of a 3.3-kVac/5-kVdc, 1.25-MW MMC employing 36 SMs and operating in the rectifier mode. Finally, Section VI concludes the article.

II. MMC BASIC OPERATING PRINCIPLES AND DEFINITION OF USED QUANTITIES

Subtraction and addition of equations formed around the loops defined in Fig. 2, for an arbitrary MMC leg, provide (1) and (2),

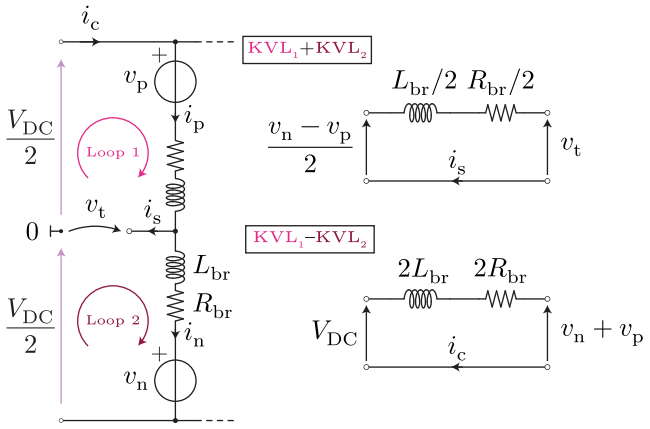

Fig. 2. MMC leg with two Kirchhoff voltage loops. Through a suitable manipulation of equations written for both loops, decoupling of the ac and dc terminal equations can be established. Henceforth, subscripts "p" and "n" will denote the upper and the lower branch quantities, respectively. Without loss of generality, no coupling between the branch inductors is assumed.

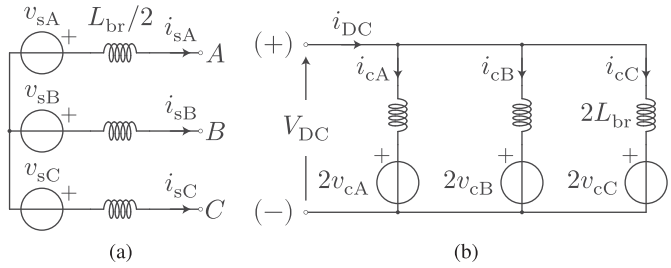

Fig. 3. MMC equivalent circuits seen from (a) ac side and (b) dc side.

from where one can note that two independent control quantities can be established

$$\frac{L_{\rm br}}{2}\frac{d}{dt}\underbrace{\left(i_{\rm p}-i_{\rm n}\right)}_{i_{\rm s}}+\frac{R_{\rm br}}{2}(i_{\rm p}-i_{\rm n})=\underbrace{\frac{v_{\rm n}-v_{\rm p}}{2}}_{v_{\rm s}}-v_{\rm t} \tag{1}$$

$$2L_{\rm br}\frac{d}{dt}\underbrace{\left(\frac{i_{\rm p}+i_{\rm n}}{2}\right)}_{i_{\rm c}}+2R_{\rm br}\frac{i_{\rm p}+i_{\rm n}}{2}=V_{\rm DC}-\underbrace{\left(v_{\rm p}+v_{\rm n}\right)}_{2v_{\rm c}}. \tag{2}$$

The difference between the upper and the lower branch current corresponds to the leg ac terminal current (3). Based on (1), it can be concluded that this current can be affected through the adjustment of the difference between the lower and the upper branch voltages labeled with $v_{\rm s}$. Repeating the procedure for all legs leads to the MMC ac-side equivalent circuit depicted in Fig. 3(a). As suggested by (2), the average value of currents flowing through the branches comprising an observed leg (4) can be controlled by means of the sum of voltages created jointly by them. Once again, establishing expression (2) for all legs results in the MMC dc-side equivalent circuit presented in Fig. 3(b). Without loss of generality, in Fig. 3(a) and (b), the

branch resistance was considered negligible

$$i_{\mathrm{s}} = i_{\mathrm{p}} - i_{\mathrm{n}} \tag{3}$$

$$i_{\mathrm{c}} = \frac{i_{\mathrm{p}} + i_{\mathrm{n}}}{2} \tag{4}$$

$$i_{\mathrm{p}} = i_{\mathrm{c}} + \frac{i_{\mathrm{s}}}{2} \tag{5}$$

$$i_{\mathrm{n}} = i_{\mathrm{c}} - \frac{i_{\mathrm{s}}}{2}. \tag{6}$$

Solving the system (3) and (4) enables a different perception of the branch currents, and according to (5) and (6), the branch current can be expressed through a suitable combination of the leg common-mode and ac terminal currents. At this point, it is important to state that the leg current component defined in (4) has been named differently within the literature so far. Although known to some as the circulating current (see, e.g., [7] and [24]), this component will henceforth be referred to as the leg common-mode current, given that circulating currents will be given another connotation. In a multiphase MMC, ac terminal currents sum up to zero under normal operating conditions. Thus, it is only the leg common-mode currents that enter the MMC dc link. For this reason, the term "circulating" was avoided in the process of naming this current component [common-mode currents leave the converter without circulating inside of it, as illustrated in Fig. 3(b)]. Since the leg-common-mode current cannot enter the ac terminal, the decoupled analysis of the leg relevant current components can be conducted.

To introduce the concept of circulating currents, one should analyze the circuit from Fig. 3(b). By means of the joint action of three legs, the current entering/leaving the dc link can be controlled. For the moment, let us assume that $v_{\mathrm{c}\{\mathrm{A/B/C}\}} = v_{\mathrm{c0}}$. On these terms, ideal distribution of the dc-link current implies that $i_{\mathrm{c}\{\mathrm{A/B/C}\}} = i_{\mathrm{DC}}/3$. Unfortunately, such a requirement is unlikely to be met for various reasons. For instance, identical impedance seen from the dc terminals cannot be guaranteed for all the legs. Therefore, expressing the leg common-mode current as the following comes in handy:

$$i_{\mathrm{c},k} = \frac{i_{\mathrm{DC}}}{3} + i_{\mathrm{c}\Delta,k}, \text{ where } \quad k = \{\mathrm{A}, \mathrm{B}, \mathrm{C}\}. \tag{7}$$

Summing the legs' common-mode currents expressed in the above manner yields

$$i_{\mathrm{c}\Delta\mathrm{A}} + i_{\mathrm{c}\Delta\mathrm{B}} + i_{\mathrm{c}\Delta\mathrm{C}} = 0. \tag{8}$$

As current components $i_{\mathrm{c}\Delta}$ do not enter the dc link (they sum up to zero), nor are they visible from the ac terminals, it can be said that they circulate inside of the MMC. For that reason, these components will henceforth be referred to as the circulating currents. In case the expression

$$v_{\mathrm{c}} = v_{\mathrm{c0}} + v_{\mathrm{c}\Delta} \tag{9}$$

holds for an observed leg, it can be shown that its circulating current can be controlled by means of the voltage component labeled with $v_{\mathrm{c}\Delta}$ [23]. However, to keep the circulating current control decoupled from the other MMC control layers, the condition

$$v_{\mathrm{c}\Delta\mathrm{A}} + v_{\mathrm{c}\Delta\mathrm{B}} + v_{\mathrm{c}\Delta\mathrm{C}} = 0 \tag{10}$$

must be satisfied at all times. Without entering into the structure of the circulating current control methods [25], it must be stressed that (10) holds only if the sum of circulating current references equals zero. In general, circulating currents can be controlled to zero; however, as will be presented in the next sections, they can be successfully used to achieve energy balancing among the converter branches. Also, injection of higher order harmonics (e.g., second) into the circulating currents with the aim of reducing the SM voltage ripple was proposed on several occasions [14], [26]–[28]. Nonetheless, this article considers the circulating current components taking part in balancing of the mean energy values, rendering the addition of higher order harmonics rather irrelevant.

By combining (9) with the fact that Fig. 3(b) presents a linear structure, the superposition principle can be applied to the MMC dc equivalent, as presented in Fig. 4. Therefore, voltage component v_{c0} affects the dc-link current/voltage, while the components $v_{\mathrm{c}\Delta\{\mathrm{A/B/C}\}}$ take part in control of the legs' circulating current components. Finally, as only two out of three circulating currents defined above are independent, one can also perceive the circulating currents as the loop currents, which was the approach adopted in [29]. However, it can be shown that circulating currents defined as such represent a linear combination of circulating currents used in [13].

III. MMC Internal Energy Balancing

Averaging the MMC leg equations over one ac-side fundamental period [6], [7], [24] leads to a straightforward connection between the leg mean energies and its ac, dc, and circulating current components. If W_{p} and W_{n} denote the average value of the total energy stored in the upper and the lower branch of an observed leg, respectively, then

$$\frac{\mathrm{d}(W_{\mathrm{p}} + W_{\mathrm{n}})}{\mathrm{d}t} = \frac{\mathrm{d}W_{\Sigma}}{\mathrm{d}t} \approx V_{\mathrm{DC}} I_{\mathrm{c}\Delta} \tag{11}$$

$$\frac{\mathrm{d}(W_{\mathrm{p}} - W_{\mathrm{n}})}{\mathrm{d}t} = \frac{\mathrm{d}W_{\Delta}}{\mathrm{d}t} \approx -\hat{v}_{\mathrm{s}} \tilde{\hat{i}}_{\mathrm{c}\Delta}. \tag{12}$$

In the above equations, $I_{\mathrm{c}\Delta}$ denotes circulating current dc part, whereas $\hat{i}_{\mathrm{c}\Delta}$ denotes the peak of the circulating current ac component being in phase with the leg ac voltage denoted by v_{s} [24]. According to (11), the dc component of the circulating current affects the total energy (Σ-energy) stored within an observed leg. Hence, it is in charge of the energy balancing in horizontal direction. On the other hand, the ac component of the circulating current affects the energy difference (Δ-energy) between two branches belonging to the same leg; therefore, it governs the vertical balancing process.

The first assumption regarding the converter energy balancing process is that it commences by calculating the circulating current components $I_{\mathrm{c}\Delta}$ and $\hat{i}_{\mathrm{c}\Delta}$ for each leg individually. However, horizontal and vertical unbalances can take any arbitrary values, meaning that simple and independent calculation of circulating currents in accordance with (11) and (12) might violate the

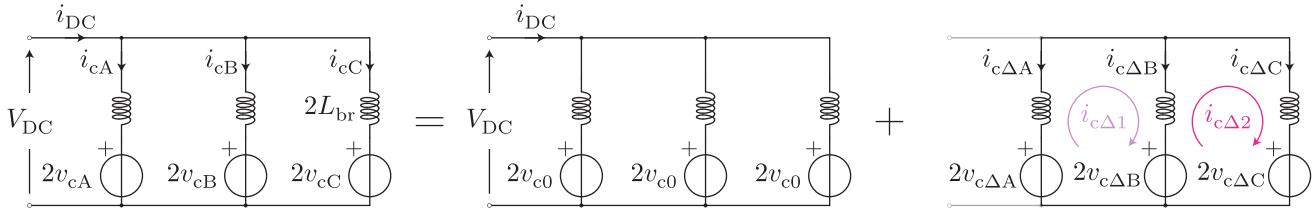

Fig. 4. Decoupling of the MMC dc-side equivalent circuit. In case voltage components $v_{\mathrm{c}\Delta}$ sum up to zero, control of circulating currents (by means of voltage components $v_{\mathrm{c}\Delta}$) remains perfectly decoupled from the control of the dc terminal current (by means of voltage component $v_{\mathrm{c}0}$).

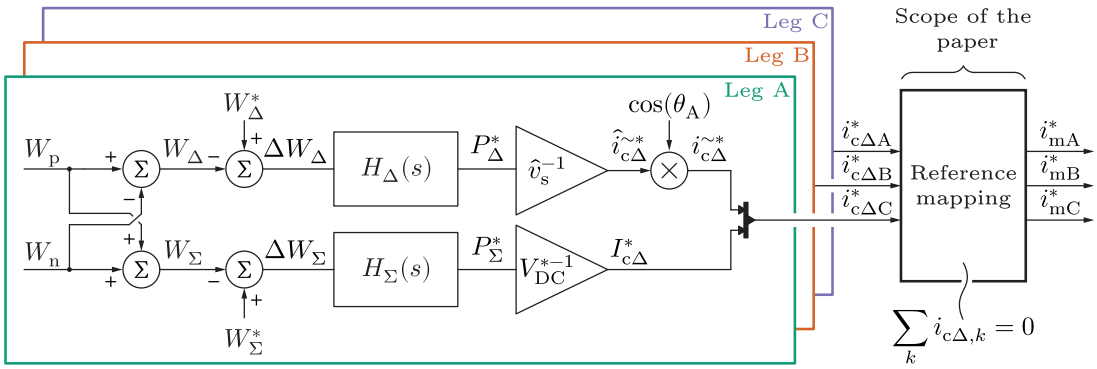

Fig. 5. Concept of generating circulating current references in the MMC. Mapping of the circulating current references generated in per-leg fashion must be performed given that individual control of the leg energies does not guarantee fulfillment of the constraint defined in (10). $H_{\Delta}(s)$ and $H_{\Sigma}(s)$ denote transfer functions of controllers being in charge of the energy balance in vertical and horizontal direction, respectively, while $v_{\mathrm{s}\{\mathrm{A/B/C}\}} = \hat{v}_{\mathrm{s}} \cos(\theta_{\{\mathrm{A/B/C}\}})$. The block named "Reference mapping" converts a set of circulating current references $i^*_{\mathrm{c\Delta}\{\mathrm{A/B/C}\}}$ into a set of new modified references $i^*_{\mathrm{m}\{\mathrm{A/B/C}\}}$ ensuring the fulfillment of (10), and its effects on the energy balancing dynamics represent the scope of this work.

condition defined in (10). Consequently, additional reference mapping, which ensures that $i^*_{\mathrm{c\Delta A}} + i^*_{\mathrm{c\Delta B}} + i^*_{\mathrm{c\Delta C}} = 0$, must be considered, as indicated in Fig. 5.

Different ways of obtaining a suitable set of circulating currents represent the scope of this article. Work in [30] contains an extensive comparison among different MMC internal control schemes. However, mapping of the circulating currents was not considered. Therefore, a theoretical gap regarding the effects the circulating currents mapping has upon the energy balancing dynamics remained unfilled. In the following paragraphs, mapping approaches used in [11]–[13] will be discussed in detail and referred to as the Methods 1–3, respectively.

A. Method 1 [11]

Even though the control of circulating current dc and ac components can be considered separately, the direction of balancing (vertical or horizontal) will be neglected as the same methodology is adopted in both cases. Therefore, results presented henceforward can be considered general.

As circulating currents were defined in the dc equivalent circuit of the MMC, their summation at the dc terminal can be formulated as

$$\underbrace{\begin{bmatrix}1 & 1 & 1\end{bmatrix}}_{T_i}\underbrace{\begin{bmatrix}i_{\mathrm{c\Delta A}} & i_{\mathrm{c\Delta B}} & i_{\mathrm{c\Delta C}}\end{bmatrix}^T}_{\vec{I}} = 0. \tag{13}$$

One can understand that matrix T_i represents the mapping $\mathbb{R}^3 \mapsto \mathbb{R}$, whereas all the vectors $\vec{I}$ being mapped to zero do not actually corrupt the MMC dc-link current (which indeed makes them circulate inside the converter). It is exactly this set of vectors that defines the null space (or kernel, hence the label $\ker(T_i)$) of matrix T_i. To put it differently, every possible combination of circulating currents must reside in the null space of T_i. Nonetheless, energy unbalances among the MMC branches/legs can take any arbitrary values resulting in the control actions violating the constraint of circulating current references summing up to zero (keep in mind that generation of circulating current references commences by performing the balancing of every leg individually). To overcome this issue, a reference vector $\vec{I}^*$, such that $T_i\vec{I}^* \neq 0$, must be projected onto the null space of T_i, resulting in a modified reference vector $\vec{I}_{\mathrm{M}}$, which ensures that (10) is always satisfied. Basically, the problem of energy balancing comes down to the identification of a suitable vector $\vec{I}_{\mathrm{M}}$, which represents the projection of the original reference $\vec{I}^*$ onto the null space of T_i, as illustrated in Fig. 6.

In general, projection of an arbitrary vector $\vec{x}$ onto an arbitrary plane/space (irrespective of its nature) means that $\vec{x}$ should actually be projected onto the basis vectors of the considered plane/space. A set of vectors $B = [\vec{b_1} \ \ldots \ \vec{b_k}]$ is called a basis of a subspace S if:

1) every vector from S can be synthesized through a linear combination of vectors from B;

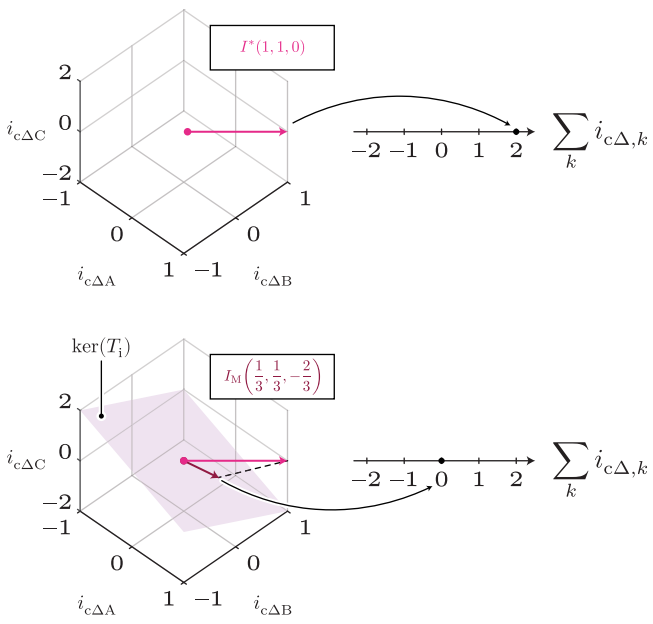

Fig. 6. Concept of generating circulating current references in the MMC in case balancing method labeled with 1 is considered. As illustrated, any reference vector $\vec{I}^* \not\subset \ker(T_i)$ must be projected onto $\ker(T_i)$ in order to guarantee the fulfillment of (10).

2) all the vectors from B are linearly independent.

Consequently, the heart of balancing strategy discussed here represents the identification of the basis vectors of $\ker(T_i)$. For this purpose, the SVD, the explanation of which can be found in [31], can be used. According to [31], any matrix can be decomposed as

$$\underset{m\times n}{T_i} = \underset{m\times m}{U} \times \underset{m\times n}{\Sigma} \times \underset{n\times n}{V^*} \tag{14}$$

where V^* represents the conjugate transpose of V. If V is real, $V^* = V^T$ is true, and (14) can be simplified as

$$\underset{m\times n}{T_i} = \underset{m\times m}{U} \times \underset{m\times n}{\Sigma} \times \underset{n\times n}{V^T}. \tag{15}$$

An important property of the SVD is that U and V are unitary (rotation) matrices, while (15) can be expanded as

$$T_i = \underset{m\times m}{\begin{bmatrix} U_{\mathrm{R}} & U_{\mathrm{N}} \end{bmatrix}} \underset{m\times n}{\begin{bmatrix} \underset{r\times r}{S} & 0 \\ 0 & 0 \end{bmatrix}} \underset{n\times n}{\begin{bmatrix} V_{\mathrm{R}}^T \\ V_{\mathrm{N}}^T \end{bmatrix}}. \tag{16}$$

From (16), it can be seen that matrix Σ contains a square $r \times r$ submatrix with elements different than zero and $n - r$ zero vectors. The number of zero vectors in Σ corresponds to the number of orthogonal vectors comprising an orthonormal basis for $\ker(T_i)$. To support such a statement, let us define $V_{\mathrm{N}} = [\vec{v}_{\mathrm{N},1} \ \ldots \ \vec{v}_{\mathrm{N},n-r}]$ and look for $T_i \times \vec{v}_{\mathrm{N},j}$, such that $1 \le j \le n - r$, as

$$T_i \times \vec{v}_{\mathrm{N},j} = \begin{bmatrix} U_{\mathrm{R}} & U_{\mathrm{N}} \end{bmatrix} \begin{bmatrix} \underset{r\times r}{S} & 0 \\ 0 & 0 \end{bmatrix} \begin{bmatrix} V_{\mathrm{R}}^T \\ V_{\mathrm{N}}^T \end{bmatrix} \vec{v}_{\mathrm{N},j}. \tag{17}$$

As all the vectors from V are orthogonal according to the definition of the SVD, $V_{\mathrm{R}}^T \vec{v}_{\mathrm{N},j} = 0_{r\times n}$, from where one can see that $T_i \vec{v}_{\mathrm{N},j} = 0$. As a result, every vector from V_{N} is in the null space of T_i. Consequently, V_{N} comprises the basis of $\ker(T_i)$ since:

1) all the vectors from V_{N} are in the null space of T_i;
2) all the vectors from V_{N} are independent (moreover, they are orthonormal);
3) the number of vectors in V_{N} corresponds to the dimension of the null space (rank-nullity theorem [31]).

Once the orthogonal basis of $\ker(T_i)$ is identified, the vector demanded by the converter balancing controllers $\vec{I}^*$ must be mapped to a suitable vector $\vec{I}_{\mathrm{M}}$. If basis vectors $V_{\mathrm{N}} = [\vec{v}_{\mathrm{N},1} \ \ldots \ \vec{v}_{\mathrm{N},n-r}]$ are at disposal, the following is to be observed at first instance:

$$V_{\mathrm{N}}^T \vec{I}^* = \begin{bmatrix} \vec{v}_{\mathrm{N},1}^T \\ \vec{v}_{\mathrm{N},2}^T \\ \vdots \\ \vec{v}_{\mathrm{N},n-r}^T \end{bmatrix} \vec{I}^* = \underbrace{\begin{bmatrix} \langle \vec{v}_{\mathrm{N},1}, \vec{I}^* \rangle \\ \langle \vec{v}_{\mathrm{N},2}, \vec{I}^* \rangle \\ \vdots \\ \langle \vec{v}_{\mathrm{N},n-r}, \vec{I}^* \rangle \end{bmatrix}}_{\text{scalar products}}. \tag{18}$$

The vector on the right-hand side of (18) contains scalar products of orthonormal basis vectors and a balancing reference vector $\vec{I}^*$. Given that $|\vec{v}_{\mathrm{N},k}| = 1$, these scalar products actually represent projections of the vector $\vec{I}^*$ onto the basis vectors from V_{N}. However, these are the coordinates of the vector $\vec{I}^*$ in a new coordinate system consisting of vectors $\vec{v}_{\mathrm{N},k}$. To obtain the coordinates of the new vector in the conventional reference frame (which actually is the vector $\vec{I}_{\mathrm{M}}$), the term $V_{\mathrm{N}}^T \vec{I}^*$ needs to be multiplied by V_{N}, resulting in

$$\vec{I}_{\mathrm{M}} = V_{\mathrm{N}} V_{\mathrm{N}}^T \vec{I}^* = \sum_{j=1}^{n-r} \vec{v}_{\mathrm{N},j} \langle \vec{v}_{\mathrm{N},j}, \vec{I}^* \rangle. \tag{19}$$

It is worthy to note that, according to [11], a previously demonstrated procedure is general, and it can be applied to any MMC-based converter. The null space of matrix T_{i} from (13) can be identified by first creating its SVD form as

$$T_i = \begin{bmatrix} 1 \end{bmatrix} \begin{bmatrix} \sqrt{3} & 0 & 0 \end{bmatrix} \sqrt{\frac{2}{3}} \begin{bmatrix} \frac{1}{\sqrt{2}} & \frac{1}{\sqrt{2}} & \frac{1}{\sqrt{2}} \\ 1 & -\frac{1}{2} & -\frac{1}{2} \\ 0 & \frac{\sqrt{3}}{2} & -\frac{\sqrt{3}}{2} \end{bmatrix}. \tag{20}$$

From here, it is straightforward to recognize that

$$V_{\mathrm{N}} = \sqrt{\frac{2}{3}} \begin{bmatrix} 1 & 0 \\ -\frac{1}{2} & \frac{\sqrt{3}}{2} \\ -\frac{1}{2} & -\frac{\sqrt{3}}{2} \end{bmatrix}. \tag{21}$$

Following (19), mapping of the circulating current references can be performed as

$$\vec{I}_{\mathrm{M}} = \begin{bmatrix} 1 & 0 & 0 \\ 0 & 1 & 0 \\ 0 & 0 & 1 \end{bmatrix} \vec{I}^* - \frac{1}{3} \begin{bmatrix} 1 & 1 & 1 \\ 1 & 1 & 1 \\ 1 & 1 & 1 \end{bmatrix} \vec{I}^*. \tag{22}$$

Fig. 7 provides graphical illustration of the balancing approach described in the previous paragraphs. As can be noted, circulating current reference modification implies the reduction

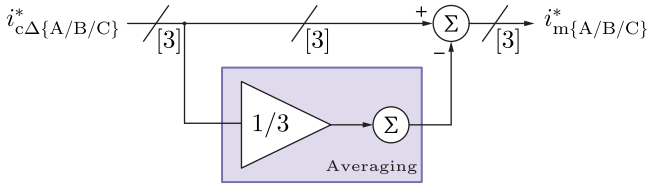

Fig. 7. Implementation of the balancing method labeled with 1.

of every individual leg reference by an average value of references generated for all the legs individually. It is important to note that the choice of the basis vectors of $\ker(T_i)$ is not unique. Any other orthogonal pair being a subset of $\ker(T_i)$ could also be chosen (see, e.g., [20]), without affecting the result obtained in (22). However, a formal proof of such a statement is omitted as, to the authors' opinion, does not increase the value of results provided above.

B. Method 2 [12]

1) Horizontal Balancing: In contrast to Method 1, where energy balancing was performed in the ABC frame, Münch *et al.* [12] propose horizontal balancing in the $\alpha\beta$ domain by means of relevant power components defined as

$$\begin{bmatrix} P_{\Sigma\alpha} \\ P_{\Sigma\beta} \end{bmatrix} = \underbrace{\sqrt{\frac{2}{3}} \begin{bmatrix} 1 & -\frac{1}{2} & -\frac{1}{2} \\ 0 & \frac{\sqrt{3}}{2} & -\frac{\sqrt{3}}{2} \end{bmatrix}}_{K_{\alpha\beta}} \begin{bmatrix} P_{\Sigma A} \\ P_{\Sigma B} \\ P_{\Sigma C} \end{bmatrix}. \tag{23}$$

Expression (11) establishes the link between power components labeled with $P_{\Sigma\{A/B/C\}}$ and their associated circulating currents $I_{c\Delta\{A/B/C\}}$, from where it is easy to see that

$$\begin{bmatrix} P_{\Sigma\alpha} \\ P_{\Sigma\beta} \end{bmatrix} = V_{DC} \begin{bmatrix} I_{c\Delta\alpha} \\ I_{c\Delta\beta} \end{bmatrix}. \tag{24}$$

Since the vector of circulating currents must remain free of any zero component, otherwise the dc-link current gets corrupted, references in the ABC domain can be obtained as

$$\begin{bmatrix} I^*_{mA} \\ I^*_{mB} \\ I^*_{mC} \end{bmatrix} = K^T_{\alpha\beta} \begin{bmatrix} I^*_{c\Delta\alpha} \\ I^*_{c\Delta\beta} \end{bmatrix}. \tag{25}$$

2) Vertical Balancing: To commence the desired analysis, one can take the case presented in Fig. 8 into consideration. As illustrated, the sum of circulating current references generated in "per-leg" fashion differs from zero. Now, let us observe phasor $\underline{i}_{c\Delta A}$ while neglecting the other two legs' balancing references. To perform the cancellation of current defined by this phasor in the dc link, two currents can be added into legs B and C. What is of crucial importance is that current components $i^A_{c\Delta B}$ and $i^A_{c\Delta C}$ do not contribute to any active power transfer in the phases they are injected to. For instance, $i^A_{c\Delta B}$ denotes the current component injected in the leg labeled with B with the aim of partially canceling the circulating current generated in leg A. As can be seen, this component is orthogonal to the ac voltage

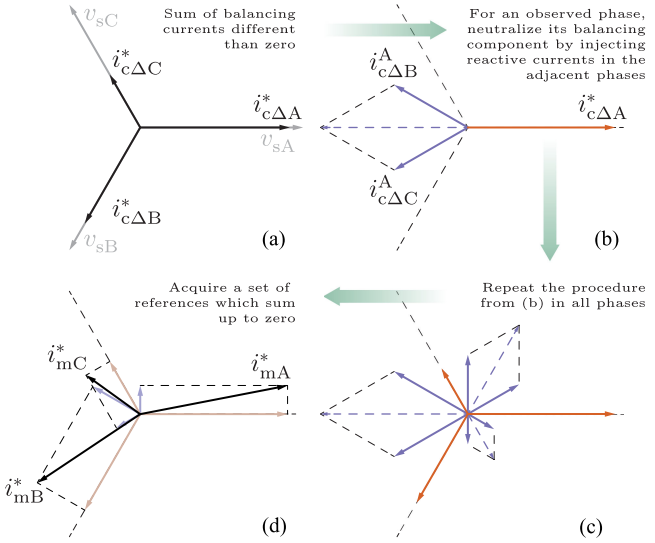

Fig. 8. Vertical balancing procedure based on the injection of orthogonal components into the circulating currents of all the legs. (a) Sum of balancing currents different than zero. (b) For an observed phase, neutralize the presence of its balancing component in the dc link by injecting reactive currents in the adjacent phases. (c) Repeat the procedure from (b) in all phases. (d) Acquire a set of references which sum up to zero.

v_{sB}. Consequently, only reactive power is generated. This is an important detail since the reactive power cannot contribute to the change of the average energy in any of the converter's branches. Finally, repeating the same procedure in the other two phases leads to the final set of circulating current references ensuring the energy balance in vertical direction.

C. Method 3 [13]

1) Horizontal Balancing: Given that Methods 2 and 3 rely on the identical principles of horizontal balancing, no further discussion is conducted on this matter.

2) Vertical Balancing: As can be seen in (21), rows of the matrix used to perform $\alpha\beta$ transformation represent the bases of $\ker(T_i)$. To a certain extent, this indicates that vertical balancing, similarly to horizontal, can be performed directly in the $\alpha\beta0$ domain by means of relevant power components being defined as

$$\begin{bmatrix} P_{\Delta\alpha} \\ P_{\Delta\beta} \\ P_{\Delta0} \end{bmatrix} = \underbrace{\sqrt{\frac{2}{3}} \begin{bmatrix} 1 & -\frac{1}{2} & -\frac{1}{2} \\ 0 & \frac{\sqrt{3}}{2} & -\frac{\sqrt{3}}{2} \\ \frac{1}{\sqrt{2}} & \frac{1}{\sqrt{2}} & \frac{1}{\sqrt{2}} \end{bmatrix}}_{K_{\alpha\beta0}} \begin{bmatrix} P_{\Delta A} \\ P_{\Delta B} \\ P_{\Delta C} \end{bmatrix}. \tag{26}$$

As already discussed, a proper control of converter's internal energies requires identification of circulating current components fulfilling this task. Given that $i_{c\Delta0} = 0$, the set of power components $P_\Delta = \{P_{\Delta\alpha}, P_{\Delta\beta}, P_{\Delta0}\}$ needs to be linked with the circulating currents expressed in the $\alpha\beta$ domain. For that purpose, two dq systems, rotating in the opposite directions,

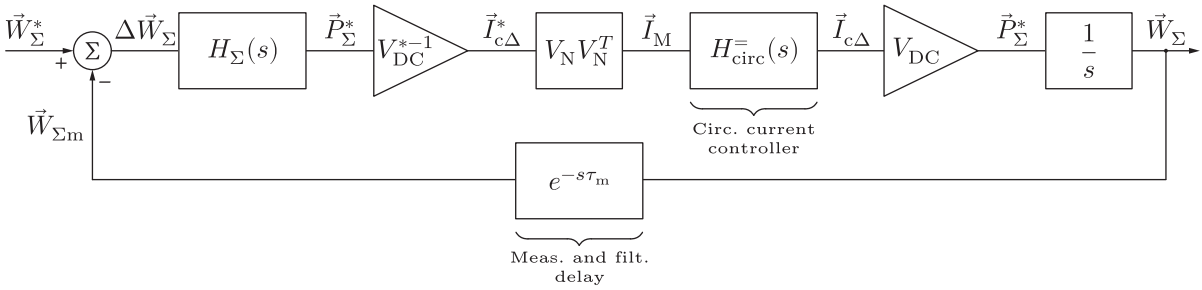

Fig. 9. Control block diagram of circulating current components maintaining the energy balance in horizontal direction (ABC domain/Method 1).

were introduced in [13], giving

$$\begin{bmatrix} i_{\rm c\Delta\alpha} \\ i_{\rm c\Delta\beta} \end{bmatrix} = \underbrace{\begin{bmatrix} \cos(\theta) & -\sin(\theta) \\ \sin(\theta) & \cos(\theta) \end{bmatrix}}_{R_+} \begin{bmatrix} i^+_{\rm c\Delta d} \\ i^+_{\rm c\Delta q} \end{bmatrix} + \underbrace{\begin{bmatrix} \cos(\theta) & \sin(\theta) \\ -\sin(\theta) & \cos(\theta) \end{bmatrix}}_{R_-} \begin{bmatrix} i^-_{\rm c\Delta d} \\ i^-_{\rm c\Delta q} \end{bmatrix} \tag{27}$$

where $\theta = \omega_{\rm s}t - \gamma$, which unveils the alignment between the dq system rotating in the counterclockwise direction and the vector of ac voltages synthesized by the MMC branches.

A set of tedious mathematical steps, which are omitted here as they can be found in [13], shows that

$$\begin{aligned} P_{\Delta\alpha} &= -\frac{2}{\sqrt{6}}\hat{v}_{\rm s} i^-_{\rm c\Delta d} \\ P_{\Delta\beta} &= +\frac{2}{\sqrt{6}}\hat{v}_{\rm s} i^-_{\rm c\Delta q} \\ P_{\Delta 0} &= -\frac{2}{\sqrt{3}}\hat{v}_{\rm s} i^+_{\rm c\Delta d} \end{aligned} \tag{28}$$

from where one can see that the component $i^+_{\rm c\Delta q}$ can be controlled to zero as it does not take part in the control of the above power components. On the other hand, a proper control of circulating current components denoted by $i^+_{\rm c\Delta d}$, $i^-_{\rm c\Delta d}$, and $i^-_{\rm c\Delta q}$ ensures balancing in the vertical direction. Furthermore, as matrix $K_{\alpha\beta 0}$ from (26) is full-rank, circulating currents in the ABC domain can be obtained as

$$\begin{bmatrix} i^{\sim *}_{\rm mA} \\ i^{\sim *}_{\rm mB} \\ i^{\sim *}_{\rm mC} \end{bmatrix} = K^T_{\alpha\beta} R_+ \begin{bmatrix} i^+_{\rm c\Delta d} \\ i^+_{\rm c\Delta q} \end{bmatrix} + K^T_{\alpha\beta} R_- \begin{bmatrix} i^-_{\rm c\Delta d} \\ i^-_{\rm c\Delta q} \end{bmatrix}. \tag{29}$$

IV. Method Comparison

A. Horizontal Balancing

Fig. 9 presents the control block diagram in case control of all the phases is performed individually (i.e., Method 1). The expression defining the vector of mapped circulating current references is

$$\vec{I}_{\rm M} = V_{\rm N} V^T_{\rm N} \frac{H_\Sigma(s)}{V^*_{\rm DC}} (\vec{W}^*_\Sigma - \vec{W}_{\Sigma\rm m}) \tag{30}$$

where $\vec{W}_\Sigma = [W_{\Sigma\rm A}\ W_{\Sigma\rm B}\ W_{\Sigma\rm C}]^T$, along with the leg total energy controller transfer function being denoted by $H_\Sigma(s)$. To establish the conditions for comparison of previously presented balancing methods, it is initially assumed that all of them rely on the identical tuning of controller $H_\Sigma(s)$. Nevertheless, identical tuning of the controllers is not mandatory, which will be discussed more in depth in the continuation of this section.

Given that the ultimate goal of the MMC control, in general sense, is to provide references for the upper and lower branch voltages, the output of the circulating current controllers is to be investigated further. In case $W^{=}_{\rm circ}(s)$ denotes the circulating current controller transfer function, voltage components $\vec{V}^*_{\rm c\Delta} = [V^*_{\rm c\Delta A}\ V^*_{\rm c\Delta B}\ V^*_{\rm c\Delta C}]^T$ can be acquired as

$$\vec{V}^*_{\rm c\Delta} = W^{=}_{\rm circ}(s)\left(\vec{I}_{\rm M} - \vec{I}_{\rm c\Delta}\right) \tag{31}$$

in case filtering and delays in the circulating current measurements are neglected. This, however, does not affect generality of results. Note that capital letters denote that dc components of quantities are analyzed in this case, which is in accordance with (11) and (12).

The matrix $V^T_{\rm N}$ represents the well-known $\alpha\beta$ transformation with the scaling coefficient equal to $\sqrt{2/3}$ [cf. (26)]; hence, (30) can be rewritten as

$$\vec{I}_{\rm M} = V_{\rm N} \frac{H_\Sigma(s)}{V^*_{\rm DC}} (\vec{W}^*_{\Sigma\alpha\beta} - \vec{W}_{\Sigma\rm m\alpha\beta}). \tag{32}$$

Substitution of (32) into (31) yields

$$\vec{V}^*_{\rm c\Delta} = W^{=}_{\rm circ}(s)\left(V_{\rm N}\frac{H_\Sigma(s)}{V^*_{\rm DC}}(\vec{W}^*_{\Sigma\alpha\beta} - \vec{W}_{\Sigma\rm m\alpha\beta}) - \vec{I}_{\rm c\Delta}\right) \tag{33}$$

while left multiplication of both sides of the above equation with $V^T_{\rm N}$ (keep in mind that $V^T_{\rm N}V_{\rm N} = I$) leads to

$$\vec{V}^*_{\rm c\Delta\alpha\beta} = W^{=}_{\rm circ}(s)\left(\frac{H_\Sigma(s)}{V^*_{\rm DC}}(\vec{W}^*_{\Sigma\alpha\beta} - \vec{W}_{\Sigma\rm m\alpha\beta}) - \vec{I}_{\rm c\Delta\alpha\beta}\right). \tag{34}$$

Expression (34) indicates that horizontal balancing, characterized by the block diagram in Fig. 9, can also be performed in the $\alpha\beta$ domain, which was actually proposed in [12] and [13]. Furthermore, expression (34) shows that irrespective of the reference frame being used for the generation of circulating current references, the obtained results are the same if identical tuning of controllers $H_\Sigma(s)$ and $W^{=}_{\rm circ}(s)$ is assumed.

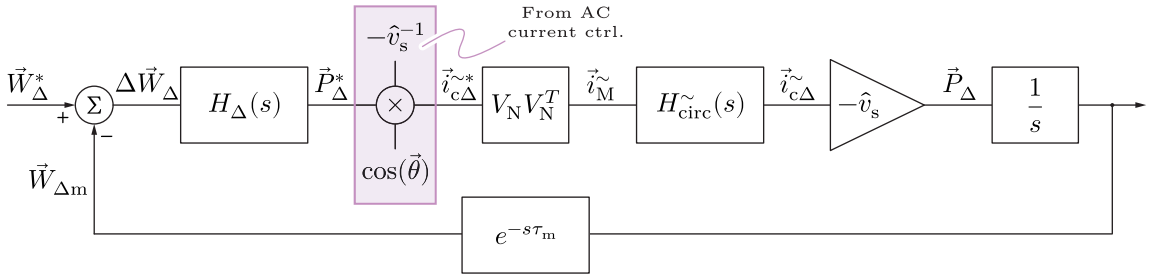

Fig. 10. Control block diagram concerning energy balancing in vertical direction (ABC frame/Method 1).

B. Vertical Balancing

As described in Section III, three vertical balancing methods rely on the use of different reference frames. Therefore, prior to commencing any further analysis, a common reference frame, from which all the methods can be observed, needs to be established. Such a step requires the extension of previously conducted analyses.

1) Method 1: By observing Fig. 10, one can note that, in contrast to the block diagram describing the horizontal balancing, vertical balancing requires the presence of nonlinear trigonometric terms presented in the form $\cos(\vec{\theta})$, where

$$\theta_{\rm A} = \omega_{\rm s} t - \gamma \tag{35}$$

$$\theta_{\rm B} = \theta_{\rm A} - \frac{2\pi}{3} \tag{36}$$

$$\theta_{\rm C} = \theta_{\rm A} + \frac{2\pi}{3} \tag{37}$$

where $\omega_{\rm s}$ and γ denote angular velocity and phase angle of voltage the MMC is synthesizing at its ac terminals, respectively. Assuming balanced load conditions, translation into the complex domain can be performed, resulting in

$$\underline{\vec{i}^{\sim}_{\rm M}} = V_{\rm N}V_{\rm N}^{T}\frac{H_{\Delta}(s)}{\hat{v}_{\rm s}}e^{-j\gamma}\underbrace{\begin{bmatrix}1 & 0 & 0\\ 0 & a^2 & 0\\ 0 & 0 & a\end{bmatrix}}_{A}\begin{bmatrix}W_{\Delta \rm A}\\ W_{\Delta \rm B}\\ W_{\Delta \rm C}\end{bmatrix} \tag{38}$$

where $a = e^{j\frac{2\pi}{3}}$. Without loss of generality, it was assumed that $\tau_{\rm m} \approx 0$, while $W^{*}_{\Delta \rm A} = W^{*}_{\Delta \rm B} = W^{*}_{\Delta \rm C} = 0$, as vertical unbalances in the legs are normally controlled to zero. Nevertheless, all the conclusions derived in the upcoming paragraphs remain the same irrespective of the choice of vertical unbalance references $W^{*}_{\Delta\{\rm A/B/C\}}$.

Mapping of the reference vector $\vec{i}^{\sim}_{\rm c\Delta}$ onto the null space of matrix $T_{\rm i}$ implies that Fortescue transformation (39) applied to (38) must output only positive and negative circulating current sequences. To put it differently, zero-sequence vector, which causes the dc-link disturbance, must be zero

$$F_{\rm pn0} = \frac{1}{3}\begin{bmatrix}1 & a & a^2\\ 1 & a^2 & a\\ 1 & 1 & 1\end{bmatrix}. \tag{39}$$

Left multiplication of (38) with (39) leads to

$$\begin{bmatrix}\underline{i}^{\sim}_{\rm m+}\\ \underline{i}^{\sim}_{\rm m-}\\ \underline{i}^{\sim}_{\rm m0}\end{bmatrix} = \frac{H_{\Delta}(s)}{\hat{v}_{\rm s}}e^{-j\gamma} \times \begin{bmatrix}\frac{1}{\sqrt{3}}W_{\Delta 0}\\ \frac{1}{\sqrt{6}}(W_{\Delta\alpha} + jW_{\Delta\beta})\\ 0\end{bmatrix} \tag{40}$$

where $W_{\alpha\beta 0} = K_{\alpha\beta 0}W_{\rm ABC}$. From (40), it can be verified that the zero component of the mapped references indeed corresponds to zero. Nevertheless, positive and negative circulating current sequences can be related to the quantities acquired by means of the $\alpha\beta$ transformation introduced in (26). Hence, the block diagram depicted on the left-hand side of Fig. 11 can be created.

2) Method 2: A straightforward way to obtain this vertical balancing method from the block diagram presented in Fig. 10 is to replace the mapping matrix $V_{\rm N}V_{\rm N}^{T}$ with another mapping matrix

$$M_{\rm m} = \begin{bmatrix}1 & j\frac{a}{\sqrt{3}} & -j\frac{a^2}{\sqrt{3}}\\ -j\frac{a^2}{\sqrt{3}} & 1 & j\frac{a}{\sqrt{3}}\\ j\frac{a}{\sqrt{3}} & -j\frac{a^2}{\sqrt{3}} & 1\end{bmatrix}. \tag{41}$$

Thereafter, by assuming that $\tau_{\rm m} \approx 0$ and $W^{*}_{\Delta\{\rm A/B/C\}} = 0$, one can establish that

$$\underline{\vec{i}^{\sim}_{\rm M}} = \frac{H_{\Delta}(s)}{\hat{v}_{\rm s}}e^{-j\gamma} \times M_{\rm m} \times \begin{bmatrix}1 & 0 & 0\\ 0 & a^2 & 0\\ 0 & 0 & a\end{bmatrix}\begin{bmatrix}W_{\Delta \rm A}\\ W_{\Delta \rm B}\\ W_{\Delta \rm C}\end{bmatrix}. \tag{42}$$

Left multiplication of both sides of (42) with $F_{\rm pn0}$ gives

$$\begin{bmatrix}\underline{i}^{\sim}_{\rm m+}\\ \underline{i}^{\sim}_{\rm m-}\\ \underline{i}^{\sim}_{\rm m0}\end{bmatrix} = \frac{H_{\Delta}(s)}{\hat{v}_{\rm s}}e^{-j\gamma} \times \begin{bmatrix}\frac{1}{\sqrt{3}}W_{\Delta 0}\\ \frac{2}{\sqrt{6}}(W_{\Delta\alpha} + jW_{\Delta\beta})\\ 0\end{bmatrix}. \tag{43}$$

3) Method 3: Translating (29) into the complex domain, followed by the left multiplication with $F_{\rm pn0}$ from (39), yields

$$\begin{bmatrix}\underline{i}^{\sim}_{\rm m+}\\ \underline{i}^{\sim}_{\rm m-}\\ \underline{i}^{\sim}_{\rm m0}\end{bmatrix} = \sqrt{\frac{2}{3}}e^{-j\gamma}\begin{bmatrix}1 & j & 0 & 0\\ 0 & 0 & 1 & -j\\ 0 & 0 & 0 & 0\end{bmatrix}\begin{bmatrix}i^{+}_{\rm c\Delta d}\\ i^{+}_{\rm c\Delta q}\\ i^{-}_{\rm c\Delta d}\\ i^{-}_{\rm c\Delta q}\end{bmatrix}. \tag{44}$$

Combining (26) and (28) with the fact that $P_{\Delta\{\alpha/\beta/0\}} = -H_{\Delta}W_{\Delta\{\alpha/\beta/0\}}$ (which is valid according

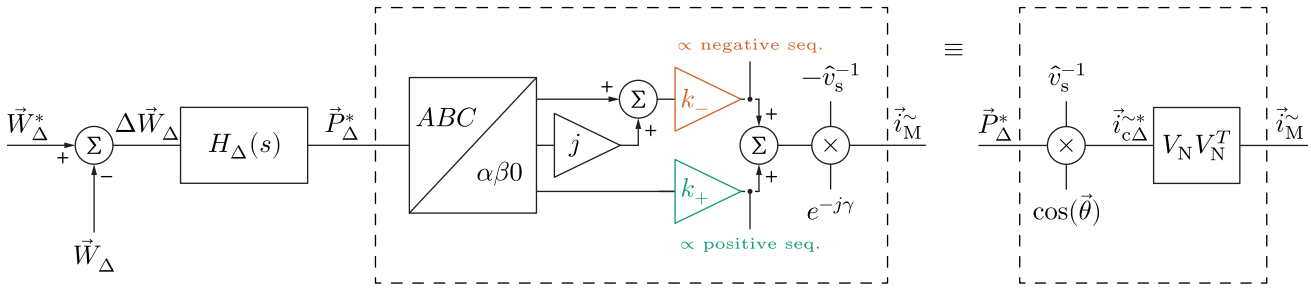

Fig. 11. Alternative way of generating circulating current references achieving the energy balance in vertical direction if balancing Method 1 is considered. Multiplication constants denoted by k_+ and k_- equal $1/\sqrt{3}$ and $1/\sqrt{6}$, respectively. The same diagram can be reused in case the other two methods are analyzed, as will be demonstrated shortly. However, the right-hand side of the figure should be discarded on these terms.

TABLE II
COEFFICIENTS DETERMINING THE METHOD USED TO MAINTAIN ENERGY BALANCE IN VERTICAL DIRECTION

	Method 1	Method 2	Method 3
k_+	$\frac{1}{\sqrt{3}}$	$\frac{1}{\sqrt{3}}$	$\frac{1}{\sqrt{2}}$
k_-	$\frac{1}{\sqrt{6}}$	$\frac{2}{\sqrt{6}}$	1

to Figs. 10 and 11, where legs' delta energy references were set as zero) along with $i^+_{\mathrm{c}\Delta\mathrm{q}} = 0$ leads to

$$\begin{bmatrix} \underline{i}^{\sim}_{\mathrm{m}+} \\ \underline{i}^{\sim}_{\mathrm{m}-} \\ \underline{i}^{\sim}_{\mathrm{m}0} \end{bmatrix} = \frac{H_\Delta(s)}{\hat{v}_\mathrm{s}} e^{-j\gamma} \times \begin{bmatrix} \frac{1}{\sqrt{2}} W_{\Delta 0} \\ W_{\Delta\alpha} + jW_{\Delta\beta} \\ 0 \end{bmatrix}. \tag{45}$$

Since the components defining the circulating current positive and negative sequences can be expressed in the form presented in Fig. 11, the values of coefficients k_+ and k_- for different balancing methods can be summarized as in Table II. As can be observed, vertical balancing methods analyzed so far differ only in terms of the multiplication constants, whereas the structure of the control block diagram illustrated on the left-hand side of Fig. 11 remains legit at all times.

Another important remark relates to the tuning of energy controllers labeled with $H_\Delta(s)$. For Methods 1 and 2, energy balancing commences for every leg individually, meaning that each leg relies on the use of its own Δ-energy controller. For every leg, this controller can be tuned differently; however, such a choice is not reasonable engineering-wise. Hence, $H_{\Delta\{\mathrm{A/B/C}\}}(s) = H_\Delta(s)$ is adopted. On the other hand, Method 3 relies on the indirect control of legs' Δ-energies through the actions being taken in the $\alpha\beta0$ domain. As α, β, and 0 axes are decoupled (orthogonal), three separate controllers can be used for each of the associated energy components. Even though identical gains can be used for all three controllers, there exists a degree of freedom allowing one to select the gains of controllers $H_{\mathrm{c}\Delta\alpha}(s)$, $H_{\mathrm{c}\Delta\beta}(s)$, and $H_{\mathrm{c}\Delta0}(s)$ differently. However, such a choice would make the upcoming comparison rather difficult to follow. Thus, it is assumed for now that $H_{\Delta\{\alpha/\beta/0\}}(s) = H_\Delta(s)$. Last but not least, the same tuning of controller $H_\Delta(s)$ is assumed for all of the methods analyzed in the next section. It must be emphasized that such a choice is not mandatory. It was rather made to provide the conditions for the comparison of three vertical balancing methods analyzed above. Nonetheless, for any other tuning of Δ-energy controllers (irrespective of the analyzed method), the analytic expressions derived above still hold, allowing one to conduct a new independent analysis.

C. Comparative Analysis

According to (40), (43), and (45), symmetrical components obtained through the Fortescue transformation of the circulating current references can be expressed as

$$\underline{i}^{\sim}_{\mathrm{m}+} = \frac{H_\Delta(s)}{\hat{v}_\mathrm{s}} e^{-j\gamma} \times k_+ W_{\Delta 0} \tag{46}$$

$$\underline{i}^{\sim}_{\mathrm{m}-} = \frac{H_\Delta(s)}{\hat{v}_\mathrm{s}} e^{-j\gamma} \times k_- (W_{\Delta\alpha} + jW_{\Delta\beta}) \tag{47}$$

while (44) can be further expanded to obtain the system

$$\begin{aligned} i^+_{\mathrm{c}\Delta\mathrm{d}} &= \Re\left(\sqrt{\frac{3}{2}} e^{j\gamma} \underline{i}^{\sim}_{\mathrm{m}+}\right), \quad i^+_{\mathrm{c}\Delta\mathrm{q}} = \Im\left(\sqrt{\frac{3}{2}} e^{j\gamma} \underline{i}^{\sim}_{\mathrm{m}+}\right) \\ i^-_{\mathrm{c}\Delta\mathrm{d}} &= \Re\left(\sqrt{\frac{3}{2}} e^{j\gamma} \underline{i}^{\sim}_{\mathrm{m}-}\right), \quad i^-_{\mathrm{c}\Delta\mathrm{q}} = -\Im\left(\sqrt{\frac{3}{2}} e^{j\gamma} \underline{i}^{\sim}_{\mathrm{m}-}\right). \end{aligned} \tag{48}$$

According to (46) and (48), circulating current component $i^+_{\mathrm{c}\Delta\mathrm{q}}$ equals zero for Methods 1 and 2 since $e^{j\gamma}\underline{i}^{\sim}_{\mathrm{m}+}$ is always a real number, whereas it is controlled to zero in case Method 3 is considered, which results in

$$\begin{aligned} i^+_{\mathrm{c}\Delta\mathrm{d}} &= \sqrt{\frac{3}{2}} k_+ \frac{H_\Delta}{\hat{v}_\mathrm{s}} W_{\Delta 0} \\ i^-_{\mathrm{c}\Delta\mathrm{d}} &= \sqrt{\frac{3}{2}} k_- \frac{H_\Delta}{\hat{v}_\mathrm{s}} W_{\Delta\alpha} \\ i^-_{\mathrm{c}\Delta\mathrm{d}} &= -\sqrt{\frac{3}{2}} k_- \frac{H_\Delta}{\hat{v}_\mathrm{s}} W_{\Delta\beta}. \end{aligned} \tag{49}$$

Systems of equations (28) and (49) can be further connected, giving

$$\begin{aligned} P_{\Delta\alpha} &= -k_- H_\Delta W_{\Delta\alpha} &&= -k_{1\alpha} H_\Delta W_{\Delta\alpha} \\ P_{\Delta\beta} &= -k_- H_\Delta W_{\Delta\beta} &&= -k_{1\beta} H_\Delta W_{\Delta\beta} \\ P_{\Delta 0} &= -\sqrt{2} k_+ H_\Delta W_{\Delta 0} &&= -k_{10} H_\Delta W_{\Delta 0}. \end{aligned} \tag{50}$$

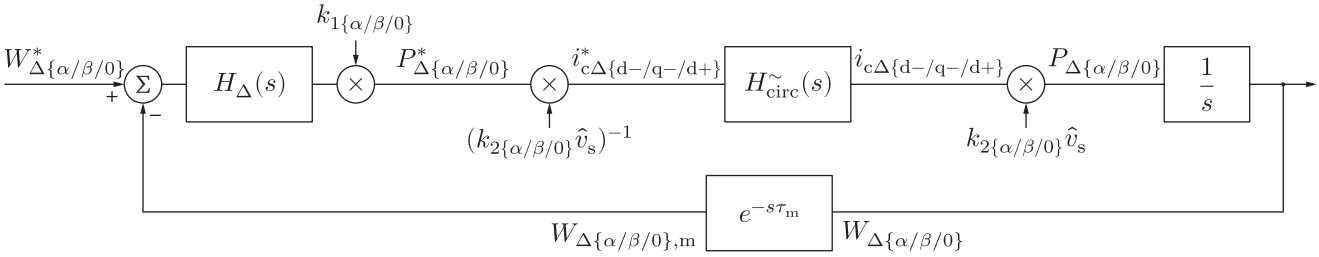

Fig. 12. General control block diagram concerning vertical balancing of the MMC energies. Coefficients $k_{1\{\alpha/\beta/0\}}$ can be read from Table III, while $k_{20} = -2/\sqrt{3}$ and $k_{2\{\alpha/\beta\}} = \mp 2/\sqrt{6}$. The advantage of the presented diagram lies in the fact that dynamic analysis of different balancing methods retains the same analytical form, with the coefficient k_1 being the only variable of interest.

TABLE III
VALUES OF COEFFICIENTS DETERMINING THE BALANCING DYNAMICS OF ENERGY COMPONENTS $W_{\Delta\alpha}$, $W_{\Delta\beta}$, AND $W_{\Delta 0}$

Coefficient	Method 1	Method 2	Method 3
$k_{1\alpha}$	$\frac{1}{2}\sqrt{\frac{2}{3}}$	$\sqrt{\frac{2}{3}}$	1
$k_{1\beta}$	$\frac{1}{2}\sqrt{\frac{2}{3}}$	$\sqrt{\frac{2}{3}}$	1
k_{10}	$\sqrt{\frac{2}{3}}$	$\sqrt{\frac{2}{3}}$	1

It is straightforward to see from the above system that the relationship between Δ-energies and relevant power components can always be found in the form of $P_{\Delta\{\alpha/\beta/0\}} = -k_{1\{\alpha/\beta/0\}} H_\Delta W_{\Delta\{\alpha/\beta/0\}}$. Table III summarizes the values of coefficients $k_{1\{\alpha/\beta/0\}}$ depending on the observed balancing method. According to (28), similar connection can be established between the $\alpha\beta 0$ power components with their associated dq current pairs as $P_{\Delta\{\alpha/\beta/0\}} = k_{2\{\alpha/\beta/0\}}\hat{v}_s i_{c\Delta\{d^-/q^-/d^+\}}$. Consequently, the control block diagram concerning energy components $W_{\Delta\{\alpha/\beta/0\}}$ can be provided in a general form, as depicted in Fig. 12. Recall that derivation of equations, presented throughout this section, assumed that $W^*_\Delta = 0$. Notwithstanding, a similar analysis could have been conducted in case W^*_Δ took any arbitrary value, which is also indicated in Fig. 12.

It can be assumed that the circulating current controller ensures aperiodic response in tracking of the negative/positive sequence references, resulting in

$$H^{\sim}_{circ}(s) = \frac{1}{1 + s\tau_c}. \tag{51}$$

Furthermore, the transfer function of the block denoting filtering and measurement of the converter energies depends on the employed control infrastructure. Nevertheless, the fact that practical values of this parameter do not exceed 1 ms in the analyzed case allows the Taylor series expansion, yielding

$$H_{mf}(s) = e^{-s\tau_m} \approx \frac{1 - s\frac{\tau_m}{2}}{1 + s\frac{\tau_m}{2}}. \tag{52}$$

The above assumptions do not hinder generality of the procedure demonstrated herewith. Conversely, in case $H_{circ}(s)$ and $H_{mf}(s)$ are found in a different form, a set of steps, similar to the one presented below, can be taken in order to conduct the comparison of different vertical balancing methods.

If the proportional controller is used, then $H_\Delta(s) = k_{p\Delta}$ leading to a straightforward analysis of the system from Fig. 12 through the root locus method. Following such a reasoning, one can define transfer function $G(s)$ as

$$G(s) = \frac{H^{\sim}_{circ}(s) H_{mf}(s)}{s} = \frac{N(s)}{D(s)} \tag{53}$$

whereas all the poles of the closed-loop transfer function formed by means of Fig. 12 satisfy the condition

$$D(s) + k_{p\Delta} k_{1\{\alpha/\beta/0\}} N(s) = 0. \tag{54}$$

According to Table III, coefficients $k_{1\{\alpha/\beta/0\}}$ can take various values depending on the observed energy component along with the adopted balancing method. For simplicity reasons, let us analyze the energy component $W_{\Delta 0}$ being controlled by means of Method 3, while the identical procedure can be followed to analyze other possible combinations.

On the above terms, $k_{10} = 1$. Thus, if $k_{p\Delta} \to 0$, zeros of the polynomial term $D(s)$, provided in (55)–(57), become poles of the transfer function W_Δ / W^*_Δ

$$\sigma_1 = 0 \tag{55}$$

$$\sigma_2 = -\frac{2}{\tau_m} \tag{56}$$

$$\sigma_3 = -\frac{1}{\tau_c}. \tag{57}$$

Similarly, if $k_{p\Delta} \to \infty$, poles of the transfer function W_Δ / W^*_Δ converge toward the zero of the polynomial term $N(s)$, which is calculated as

$$n_1 = \frac{2}{\tau_m}. \tag{58}$$

At this point, the root locus can be constructed; however, time constants τ_m and τ_c can stand in an arbitrary order (e.g., $\tau_m > \tau_c$ and *vice versa*). Therefore, to facilitate the root locus construction, parameters of the industrial controller, employed as described in Section V, will be relied on. Namely, in case bandwidth of the circulating current controller is assumed to match the cutoff frequency of the transfer function $H^{\sim}_{circ}$, then

$$\tau_c = \frac{1}{2\pi f_{bw,circ}}. \tag{59}$$

TABLE IV
PARAMETERS OF THE CONVERTER USED FOR RESULTS VERIFICATION PURPOSE

Rated power (S^*)	Output voltage (V_{DC})	Grid voltage (v_{g})	Number of SMs per branch (N)	Nominal SM voltage (V_{SM})	SM capacitance (C_{SM})	Branch inductance (L_{br})	Branch resistance (R_{br})	PWM carrier frequency (f_{c})	Fundamental frequency (f_{o})
1.25MVA	5kV	3.3kV	6	1kV	3.36mF	2.5mH	60mΩ	1kHz	60Hz

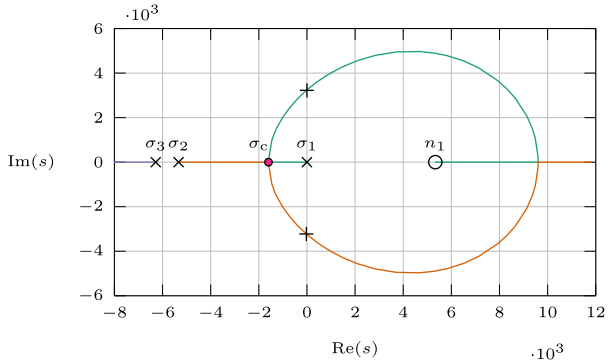

Fig. 13. Root locus constructed based on the function $G(s)$ from (53).

In the setup used for verification purposes, $f_{\mathrm{bw,circ}} \approx 1\mathrm{kHz}$ was achieved. Without entering into the structure of the employed controller, the time required for it to obtain the information on the MMC SMs voltage measurements can be approximated as $\tau_{\mathrm{m}} \approx 375\ \mu\mathrm{s}$.

From here, the desired root locus can be constructed as in Fig. 13. Increasing the value of parameter $k_{\mathrm{p}\Delta}$ causes the poles denoted by σ_1 and σ_2 to approach each other all until a critical point σ_{c}, after which these poles slowly start to move toward the right half-plane, is reached. It is important to note that, before this point is reached, σ_1 represents the most dominant pole in the system; thus, it determines its dynamic. In other words, the further the pole σ_1 from the imaginary axis, the faster the system response (under the assumption of $\sigma_1 > \sigma_{\mathrm{c}}$). To calculate the value $k^*_{\mathrm{p}\Delta}$ at which $\sigma_1 = \sigma_2 = \sigma_c$, one can substitute the solution of

$$D'(s)N(s) - N'(s)D(s) = 0 \tag{60}$$

which is actually $s = \sigma_{\mathrm{c}}$, into

$$k^*_{\mathrm{p}\Delta} = -\frac{D(\sigma_{\mathrm{c}})}{N(\sigma_{\mathrm{c}})}. \tag{61}$$

Given that (61) represents an expression being quite cumbersome, its analytic form is omitted; however, for recently adopted parameters τ_{c} and τ_{m}, it can be calculated that $k^*_{\mathrm{p}\Delta} \approx 642$. To investigate whether $k^*_{\mathrm{p}\Delta}$ falls within any realistic range, one can rely on the parameters of an exemplary converter provided in Table IV. In this case, nominal value of the total branch energy can be calculated as $W^*_{\mathrm{br}} \approx C_{\mathrm{SM}} V^{*2}_{\mathrm{br}\Sigma}/(2\,N)$. As an example, one can adopt $\Delta W_{\Delta[\mathrm{p.u}]} = 10\%$ in order to calculate that, on these terms,

$$\hat{i}_{\mathrm{c}\Delta 0} = k_{\mathrm{p}\Delta}\frac{0.1\sqrt{3}W^*_{\mathrm{br}}}{2\hat{v}_{\mathrm{s}}} \approx 210\ \mathrm{A} \tag{62}$$

which is approximately 70% of the converter nominal ac current amplitude. From the MMC hardware design standpoint, such a high value of the circulating current is unacceptable, as it would demand heavy converter oversizing. From the control aspect, on the other hand, maximal values of the circulating current can be limited by the saturation blocks. However, with the proportional gain values as high as $k^*_{\mathrm{p}\Delta}$, the system will always operate in the saturation, making it nonlinear. Therefore, practical values of the gain $k_{\mathrm{p}\Delta}$ must be set to a significantly lower value compared to the one guaranteeing the fastest aperiodic response ($k_{\mathrm{p}\Delta} \ll k^*_{\mathrm{p}\Delta}$). What is more, the same conclusion could be made for all the balancing methods considered in this article, as well as all of the energy components $W_{\Delta\{\alpha/\beta/0\}}$.

So far, identical tuning of the Δ-energy controller has been adopted for all of the analyzed methods. If so, one can note that irrespective of the observed energy component $W_{\Delta\{\alpha/\beta/0\}}$, the distance between the dominant pole and imaginary axis in the s-plane increases proportionally with the coefficients $k_{1\{\alpha/\beta/0\}}$ (keep in mind that $k_{\mathrm{p}\Delta}$ is fixed). According to Table III, these coefficients stand in the ascending order if moving from methods labeled with 1 to 3. This means that, for the identical values of P-controller gain, Method 3 is expected to provide the fastest balancing of energies in vertical direction, at least if $k_{\mathrm{p}\Delta} \ll k^*_{\mathrm{p}\Delta}$ holds.

Notwithstanding, identical tuning of energy controllers for all the methods is not mandatory, as already discussed above. Namely, Method 3 implies independent (decoupled) control of energy components in the $\alpha\beta 0$ frame. Consequently, the gains of controllers $H_{\mathrm{c}\Delta\alpha}(s)$, $H_{\mathrm{c}\Delta\beta}(s)$, and $H_{\mathrm{c}\Delta 0}(s)$ can be selected differently. According to (54), the parameter determining the position of poles in the transfer function $W_{\Delta\{\alpha/\beta/0\}}/W^*_{\Delta\{\alpha/\beta/0\}}$ equals $k_{\mathrm{p}\Delta}k_{1\{\alpha/\beta/0\}}$. Consequently, the dynamics guaranteed by Methods 1 and 2 can be obtained through the use of Method 3 in case tuning of the controllers according to the following is performed

$$H^{(\text{method 3})}_{\mathrm{c}\Delta 0} = H^{(\text{method 1/2})}_{\Delta} \times \frac{k^{(\text{method 1/2})}_{10}}{k^{(\text{method 3})}_{10}} \tag{63}$$

$$H^{(\text{method 3})}_{\mathrm{c}\Delta\{\alpha/\beta\}} = H^{(\text{method 1/2})}_{\Delta} \times \frac{k^{(\text{method 1/2})}_{1\{\alpha/\beta\}}}{k^{(\text{method 3})}_{1\{\alpha/\beta\}}}. \tag{64}$$

From Table III, it can be seen that the ratio between coefficients $k_{1\{\alpha/\beta/0\}}$ for Methods 2 and 3 equals $\sqrt{2/3}$. This indicates that multiplying the gain $k_{\mathrm{p}\Delta}$ by $\sqrt{3/2}$, in case Method 2 is considered, leads to the same Δ-energy dynamics as if Method 3 is used. Nonetheless, the same cannot be claimed for Method 1. Namely, it can be seen from the first and the third column of Table III that the ratio of coefficients $k_{1\{\alpha/\beta/0\}}$

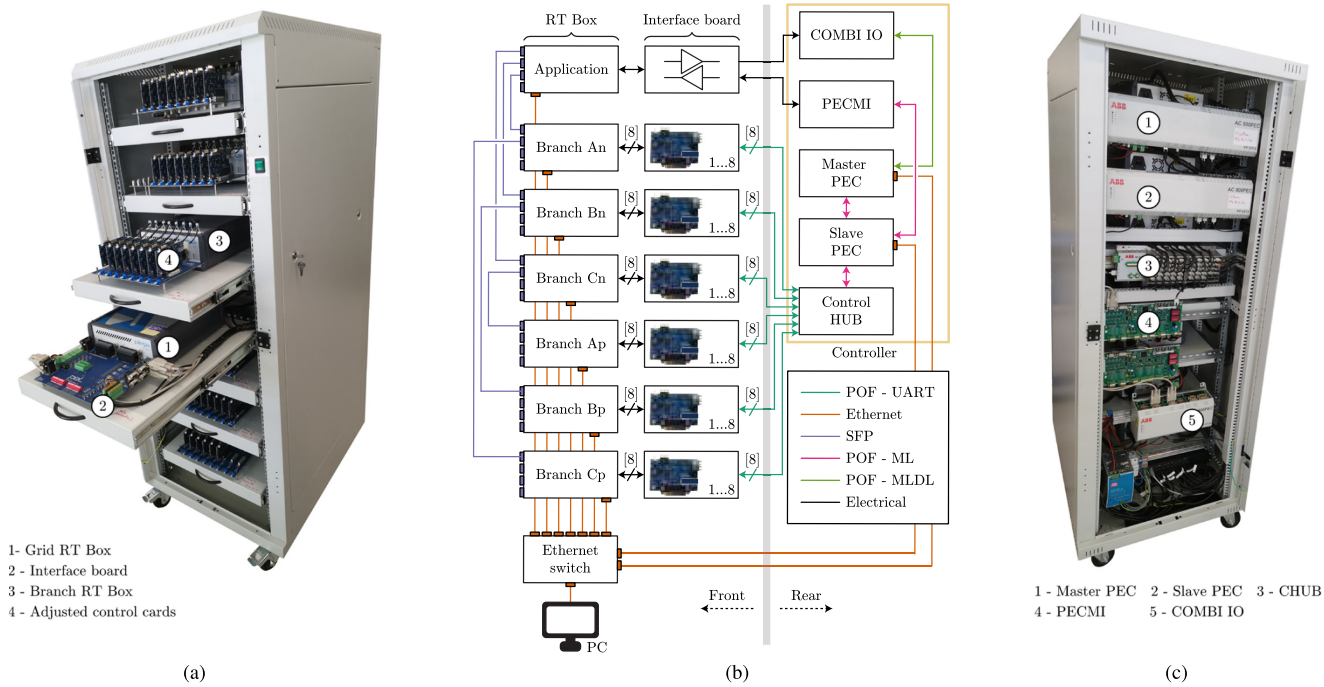

(a) (b) (c)

Fig. 14. HIL system employed to validate the results presented throughout this article. (a) Front view. (b) Wiring diagram. (c) Rear view.

changes depending on the observed axis (α, β, or 0). For example, multiplying the gain $k_{\mathrm{p}\Delta}$ by $\sqrt{3/2}$ leads to the response guaranteed by Method 3; however, only in the case of $W_{\Delta 0}$ component. Δ-energy response in the α and β axes would still remain slower compared to Method 3 given that the ratio of products $k_{\mathrm{p}\Delta}k_{1\{\alpha/\beta\}}$ for Methods 1 and *3* remains equal to $1/2$ on these terms. Similar analysis can be conducted in case identical response in α/β axes is to be obtained for Methods 1 and *3*. However, the same dynamic response cannot be ensured for the $W_{\Delta 0}$ component.

It must be emphasized that the aim of the above discussion is not to determine what balancing method provides the best performance. On the contrary, the analytic relationships among the chosen methods are provided, outlining the ability, but also the inability in certain cases, to obtain the identical dynamic responses irrespective of the employed balancing method. Consequently, the freedom to choose the balancing method of preference is completely left to the control engineer dealing with this subject. Last but not least, throughout the whole analysis conducted above, $\alpha\beta$ transformation with coefficient $C_{\alpha\beta} = \sqrt{2/3}$ was used. Nevertheless, for Methods 2 and 3, another choice of coefficients (e.g., $2/3$ or even 1) can be made. In that case, the same analysis can be conducted, however, with the second and third columns from Table II being multiplied by either $\sqrt{2/3}$ ($C_{\alpha\beta} = 2/3$) or $\sqrt{3/2}$ ($C_{\alpha\beta} = 1$).

V. HIL Verification

As presented in Fig. 14(a), the setup used for HIL verification purpose comprises seven RT-Boxes [32] provided by Plexim. In addition, 48 SM cards, out of which 36 are used in this case, hosting the DSP and logical circuitry of the real MMC SM described in [33] were interfaced with six RT-Boxes, each containing the model of an MMC branch. Seventh RT Box [fourth from the top in Fig. 14(a)] contains the model of a grid the converter is connected to, along with the auxiliary signals which are irrelevant for the scope of this article. In Fig. 14(c), two ABB PEC800 controllers can be recognized, and they are connected in the master–slave structure. The main reason for such a configuration lies in the fact that several of these HIL systems can be connected to operate in various configurations (series–parallel MMCs). Therefore, each slave controller is assigned the task of controlling its associated MMC, while one master controller is to handle general (application) state machine and references. Other parts of the system visible in Fig. 14(c) are in charge of the voltage/current measurements (PECMI), distribution of optical signals (CHUB), and manipulation of relays, switches, and other user defined arbitrary signals (COMBIO). It is important to note that the identical control structure is used in the real MMC prototype making all of the presented results realistic.

Normal operating conditions of the MMC imply that the Σ- and Δ-energies are controlled to $W_{\Sigma} = 1$ p.u and $W_{\Delta} = 0$ p.u. Testing of the energy controller responses requires the MMC to be found in a state with the energies deviating from the above setpoints. However, equivalent conclusions can be made in case relevant unbalances are intentionally created. Therefore, three different unbalance scenarios were defined, as will be seen shortly. The power processed by the analyzed MMC was set to the nominal value, which is, along with the other converter properties, provided in Table IV. For all of the inspected balancing methods, energy controllers were tuned identically as $k_{\mathrm{p}\{\Sigma/\Delta\}} = 50$. Finally, as vertical and horizontal balancing represent two decoupled problems, they are treated separately.

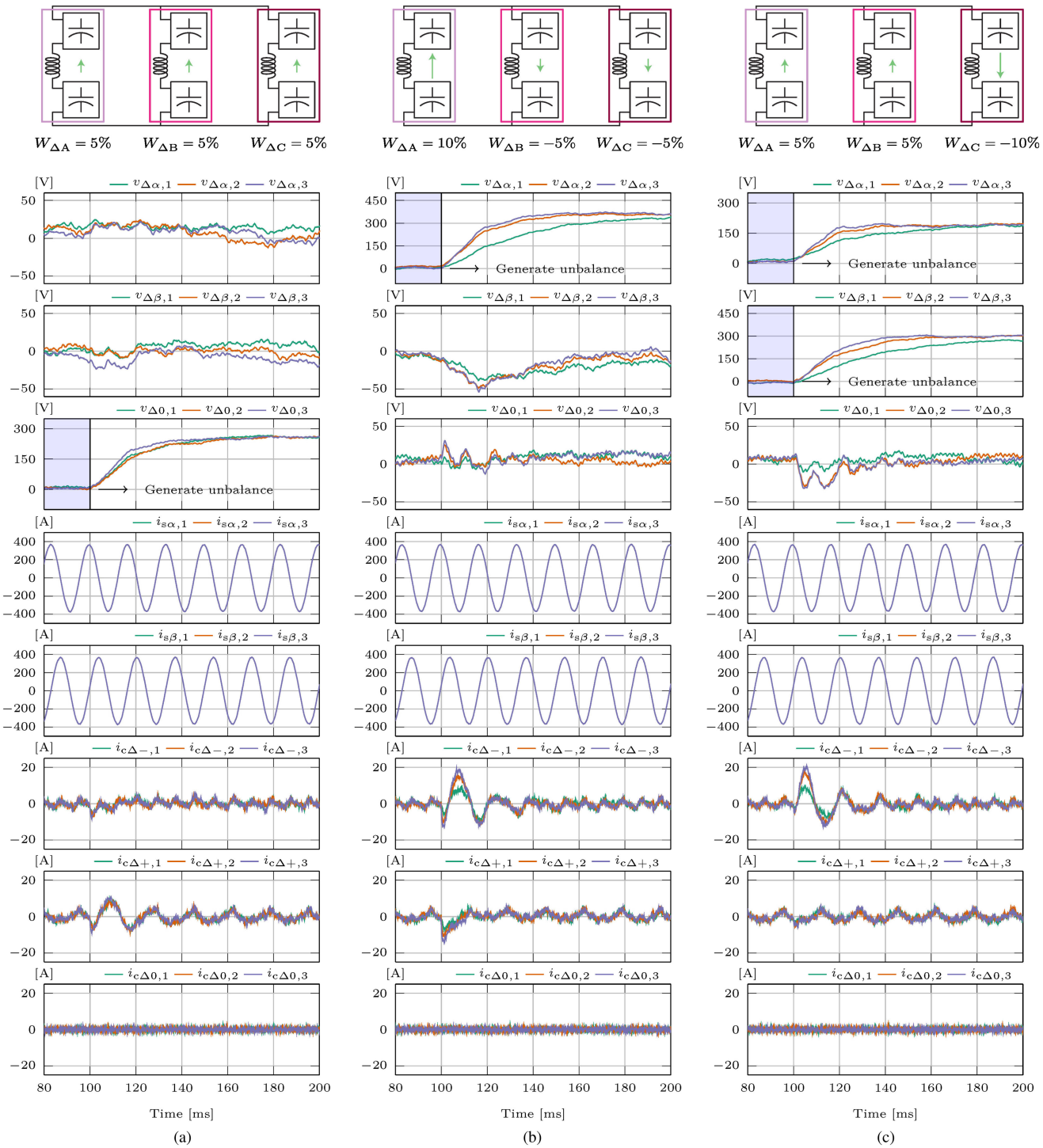

Fig. 15. Results acquired through the use of HIL setup for the cases of three different unbalance scenarios in vertical direction. (a) Scenario 1. (b) Scenario 2. (c) Scenario 3.

A. *Vertical Balancing*

Fig. 15 presents waveforms relevant for comparison of three balancing methods in case vertical unbalance scenarios labeled with 1, 2, and 3 are observed. As branch voltages are actually the quantity being measurable, while energies represent a quantity requiring calculation, the desired comparison includes Σ- and Δ- leg voltages. Nevertheless, validity of the upcoming conclusions is not affected by such a metrics. To facilitate the comparison, Σ and Δ voltage components were observed through their α, β, and 0 components, while subscripts 1, 2, and 3 relate a presented waveform with the balancing method it is associated with. In case the MMC processes any power, total

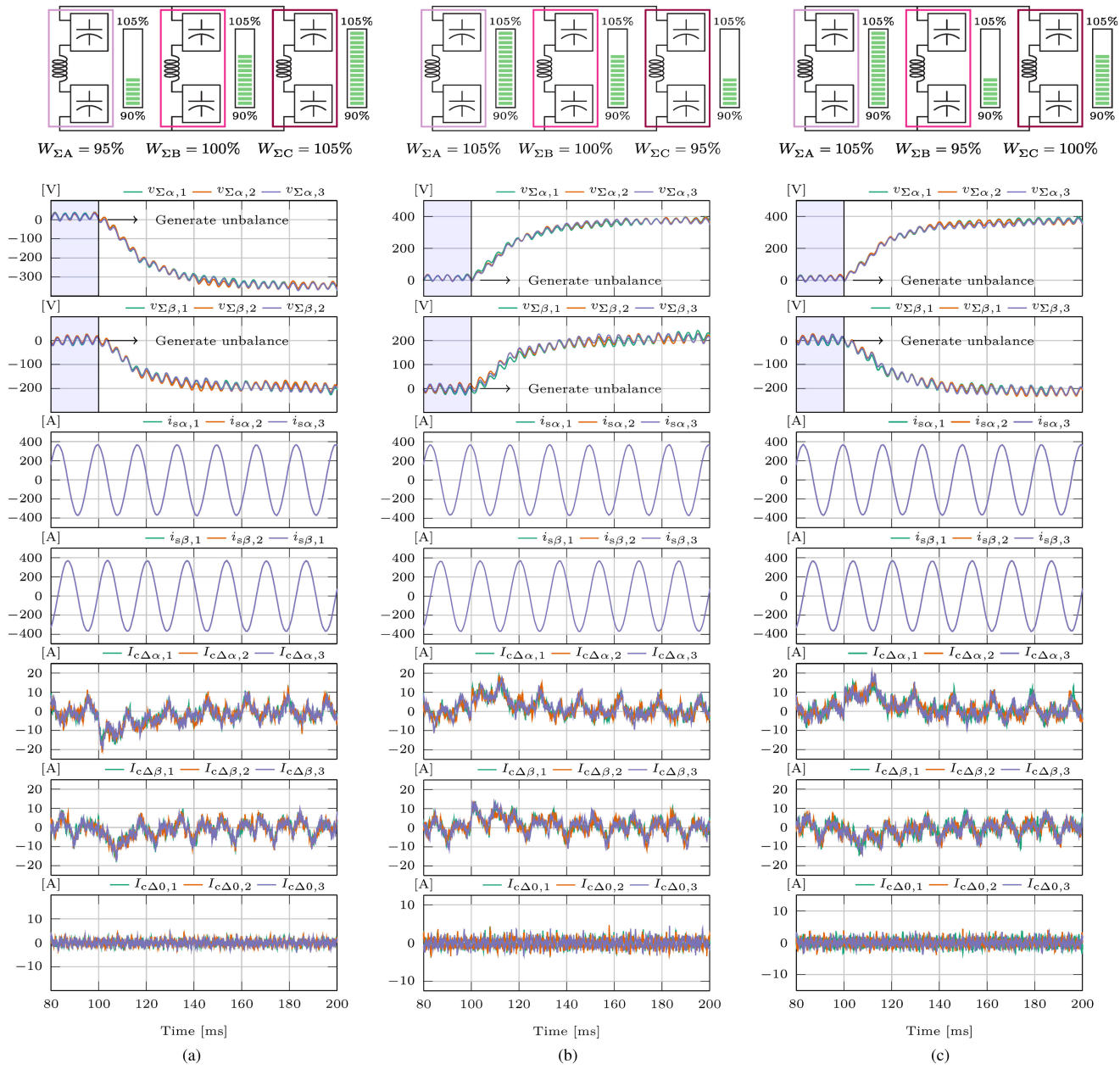

Fig. 16. Results acquired through the use of HIL setup for the cases of three different unbalance scenarios in horizontal direction. (a) Scenario 1. (b) Scenario 2. (c) Scenario 3.

branch voltages in all the phases feature inevitable oscillations. However, for the sake of presenting how the mean branch/leg energies change, depending on the employed balancing strategy, these oscillations were filtered out from the obtained waveforms.

Fig. 15(a) provides the waveforms obtained from the employed HIL setup in case identical unbalances are generated in each leg. Consequently, it is evident that the only component being affected is $v_{\Delta 0}$. According to Table III and (50), when the voltage/energy component $v_{\Delta 0}/W_{\Delta 0}$ is investigated, Methods 1 and 2 are supposed to provide identical response as, in both cases, $k_{10} = \sqrt{2/3}$. The third plot from the top validates such a statement. However, Method 3 provides faster response than two latter methods, which is perfectly aligned with the analyses conducted in Section IV-C.

An important detail that one should always keep in mind is that energy balancing inside the MMC represents an internal matter, meaning that it should never be observed from ac and dc terminals. As can be seen from Fig. 15(a)–(c), intentional generation of Δ-energy (voltage) unbalances does not affect the ac terminal currents, expressed through the Clarke transformation as $i_{s\{\alpha/\beta\}}$.

Furthermore, expression (28) establishes the link between the power components in the $\alpha\beta 0$ frame and circulating current positive/negative sequences. Accordingly, positive sequence of

circulating current, denoted by $i_{c\Delta,+}$, controls the voltage unbalance component being common for all three legs ($v_{\Delta 0}$), while negative and zero components get controlled to zero, as can be confirmed from the last three plots in Fig. 15(a). A very important remark refers to the absence of the circulating current component $i_{c\Delta 0}$. Namely, as long as the sum of circulating currents equals zero, no disturbance of the dc-link current occurs, which is the main purpose of balancing methods addressed in this work.

Fig. 15(b) takes another unbalance scenario into account. According to Section IV-C, Method 3 is expected to provide the fastest energy reference tracking in case α and β unbalances are to be generated or suppressed. Such a statement can easily be confirmed from the top-most plot of Fig. 15(b). An important detail to be noted refers to the relationship between the negative sequence of circulating currents is in case Methods 1 and 2 are compared. From (40) and (43), one can realize that Method 2 requires negative sequence of circulating current being twice as high compared to the one demanded by Method 1, which is observable from the third plot from the bottom of Fig. 15(b). Finally, Fig. 15(c) presents the case where both α and β voltage/energy unbalances are generated. As expected, the speed of response increases as moving from methods labeled with 1 to 3, if identical tuning of energy controllers is relied on. However, such a constraint does not have to be necessarily respected, and desired dynamics can be obtained for all the systems through manipulation of Σ- or Δ-energy controller gains, as suggested in (63) and (64).

B. Horizontal Balancing

Fig. 16 provides waveforms relevant for comparison of three balancing methods in case horizontal unbalance scenarios labeled with 1, 2, and 3 are observed. According to Section IV-A, all of the horizontal balancing methods considered above should provide the same response in case unbalances in horizontal direction are to be generated or suppressed. This statement is easily verifiable through Fig. 16(a)–(c). Identically to Fig. 15, ac terminal currents remain unaffected by the actions of the energy balancing controllers. According to (24), generation/suppression of an unbalance in the α/β component of the legs' Σ- energies requires generation of circulating current dc components $I_{c\Delta\alpha}$ and $I_{c\Delta\beta}$, respectively. Such a statement can be confirmed from Fig. 16(a)–(c). Finally, decoupling from the control of the dc-link current can be verified through the fact that the sum (zero component) of the circulating currents, labeled with $I_{c\Delta 0}$, equals zero in all of the analyzed cases.

VI. Conclusion

In this article, the unprecedented connection among three basic MMC energy balancing methods was established, and all the results were verified on the large-scale HIL setup employing a real industrial controller. Mathematical reinforcement of the method relying on the use of the SVD was provided, bringing it closer to the engineering community. Under the assumption of identical energy controller tuning, all of the analyzed methods provide the same performance from the standpoint of horizontal balancing. However, in case energy balancing in vertical direction is considered, the way circulating current references are mapped onto the null space of matrix describing the circulating currents summation in the dc link has a significant impact upon the balancing system dynamics. Nonetheless, it was shown that a suitable tuning controller gains allows one to shape the Δ-energy dynamic response, irrespective of the used balancing method. Therefore, the choice of the preferred vertical balancing method is to be made by the MMC control designer.

References

[1] A. Lesnicar and R. Marquardt, "An innovative modular multilevel converter topology suitable for a wide power range," in Proc. *IEEE Bologna Power Tech. Conf.*, Jun. 2003, vol. 3, p. 6.

[2] M. Glinka and R. Marquardt, "A new ac/ac-multilevel converter family applied to a single-phase converter," in *Proc. 5th Int. Conf. Power Electron. Drive Syst.*, Nov. 2003, vol. 1, pp. 16–23.

[3] C. Oates, "A methodology for developing 'chainlink' converters," in *Proc. 13th Eur. Conf. Power Electron. Appl.*, 2009, pp. 1–10.

[4] A. Nami, J. Liang, F. Dijkhuizen, and G. D. Demetriades, "Modular multilevel converters for HVDC applications: *Review converter cells functionalities*," *IEEE Trans. Power Electron.*, vol. 30, no. 1, pp. 18–36, Jan. 2015.

[5] S. Heinig, "Main circuits, submodules, and auxiliary power concepts for converters in HVDC grids," Ph.D. dissertation, School Elect. Eng. Comput. Sci., KTH Royal Institute of Technology, Stockholm, Sweden, 2020.

[6] A. Antonopoulos, L. Angquist, and H.-P. Nee, "On dynamics and voltage control of the modular multilevel converter," in *Proc. 13th Eur. Conf. Power Electron. Appl.*, 2009, pp. 1–10.

[7] L. Harnefors, A. Antonopoulos, S. Norrga, L. Angquist, and H. Nee, "Dynamic analysis of modular multilevel converters," *IEEE Trans. Ind. Electron.*, vol. 60, no. 7, pp. 2526–2537, Jul. 2013.

[8] A. Zama, S. A. Mansour, D. Frey, A. Benchaib, S. Bacha, and B. Luscan, "A comparative assessment of different balancing control algorithms for modular multilevel converter (MMC)," in *Proc. 18th Eur. Conf. Power Electron. Appl.*, 2016, pp. 1–10.

[9] H. A. Pereira *et al.*, "Capacitor voltage balance performance comparison of MMC-statcom using NLC and PS-PWM strategies during negative sequence current injection," in *Proc. 18th Eur. Conf. Power Electron. Appl.*, 2016, pp. 1–9.

[10] L. Mathe, "Performance comparison of the modulators with balancing capability used in MMC applications," in *Proc. IEEE 26th Int. Symp. Ind. Electron.*, 2017, pp. 815–820.

[11] A. J. Korn, M. Winkelnkemper, P. Steimer, and J. W. Kolar, "Capacitor voltage balancing in modular multilevel converters," in *Proc. 6th IET Int. Conf. Power Electron., Mach. Drives*, Mar. 2012, pp. 1–5.

[12] P. Münch, D. Görges, M. Izák, and S. Liu, "Integrated current control, energy control and energy balancing of modular multilevel converters," in *Proc. 36th Annu. Conf. IEEE Ind. Electron. Soc.*, Nov. 2010, pp. 150–155.

[13] J. Kolb, F. Kammerer, M. Gommeringer, and M. Braun, "Cascaded control system of the modular multilevel converter for feeding variable-speed drives," *IEEE Trans. Power Electron.*, vol. 30, no. 1, pp. 349–357, Jan. 2015.

[14] G. Bergna *et al.*, "An energy-based controller for HVDC modular multilevel converter in decoupled double synchronous reference frame for voltage oscillation reduction," *IEEE Trans. Ind. Electron.*, vol. 60, no. 6, pp. 2360–2371, Jun. 2013.

[15] H. Fehr and A. Gensior, "Improved energy balancing of grid-side modular multilevel converters by optimized feedforward circulating currents and common-mode voltage," *IEEE Trans. Power Electron.*, vol. 33, no. 12, pp. 10903–10913, Dec. 2018.

[16] H. Fehr and A. Gensior, "Eigenvalue optimization of the energy-balancing feedback for modular multilevel converters," *IEEE Trans. Power Electron.*, vol. 34, no. 11, pp. 11482–11495, Nov. 2019.

[17] M. Utvic and D. Dujic, "Generalized theory on direct arm energy control in modular multilevel converters," *CPSS Trans. Power Electron. Appl.*, vol. 5, no. 4, pp. 388–399, Dec. 2020.

[18] K. Shinoda, J. Freytes, A. Benchaib, J. Dai, H. Saad, and X. Guillaud, "Energy difference controllers for MMC without dc current perturbations," in *Proc. 2nd Int. Conf. HVDC*, 2016.

[19] S. Cui, S. Kim, J. Jung, and S. Sul, "A comprehensive cell capacitor energy control strategy of a modular multilevel converter (MMC) without a stiff dc bus voltage source," in *Proc. IEEE Appl. Power Electron. Conf. Expo.*, 2014, pp. 602–609.
[20] M. Basić, S. Milovanović, and D. Dujić, "Comparison of two modular multilevel converter internal energy balancing methods," in *Proc. 20th Int. Symp. Power Electron.*, 2019, pp. 1–8.
[21] F. Kammerer, J. Kolb, and M. Braun, "Fully decoupled current control and energy balancing of the modular multilevel matrix converter," in *Proc. 15th Int. Power Electron. Motion Control Conf.*, Sep. 2012, pp. *LS2a.3-1–LS2a.3-8*.
[22] S. Milovanović and D. Dujić, "On facilitating the modular multilevel converter power scalability through branch paralleling," in *Proc. IEEE Energy Convers. Congr. Expo.*, Sep. 2019, pp. 6875–6882.
[23] S. Milovanovic, "MMC-based conversion for MVDC applications," p. 268, 2020. [Online]. Available: http://infoscience.epfl.ch/record/277121
[24] K. Sharifabadi, L. Harnefors, H.-P. Nee, S. Norrga, and R. Teodorescu, *Design, Control, and Application of Modular Multilevel Converters for HVDC Transmission Systems*. Hoboken, NJ, USA: Wiley, 2016.
[25] A. Christe and D. Dujic, "Modular multilevel converter control methods performance benchmark for medium voltage applications" *IEEE Trans. Power Electron*, vol. 34, no. 5, pp. 4967–4980, May 2018.
[26] A. Rasic, U. Krebs, H. Leu, and G. Herold, "Optimization of the modular multilevel converters performance using the second harmonic of the module current," in *Proc. 13th Eur. Conf. Power Electron. Appl*., Sep. 2009, pp. 1–10.
[27] J. Pou, S. Ceballos, G. Konstantinou, V. G. Agelidis, R. Picas, and J. Zaragoza, "Circulating current injection methods based on instantaneous information for the modular multilevel converter," *IEEE Trans. Ind. Electron.*, vol. 62, no. 2, pp. 777–788, Feb. 2015.
[28] X. Li, Q. Song, W. Liu, S. Xu, Z. Zhu, and X. Li, "Performance analysis and optimization of circulating current control for modular multilevel converter," *IEEE Trans. Ind. Electron.*, vol. 63, no. 2, pp. 716–727, Feb. 2016.
[29] D. Karwatzki and A. Mertens, "Generalized control approach for a class of modular multilevel converter topologies," *IEEE Trans. Power Electron.*, vol. 33, no. 4, pp. 2888–2900, Apr. 2018.
[30] S. Wang, G. P. Adam, A. M. Massoud, D. Holliday, and B. W. Williams, "Analysis and assessment of modular multilevel converter internal control schemes," *IEEE Trans. Emerg. Sel. Topics Power Electron.*, vol. 8, no. 1, pp. 697–719, Mar. 2020.
[31] G. Strang, *Linear Algebra and Its Applications, London, U.K.: Thomson Learning*, 1988.
[32] *Simulation Platform for Power Electronics Systems*, Accessed: Nov. 21, 2020. [Online]. Available: https://www.plexim.com/sites/default/files/rtboxmanual.pdf
[33] M. Utvic, I. P. Lobos, and D. Dujic, "Low voltage modular multilevel converter submodule for medium voltage applications," in *Proc. PCIM Eur.Int. Exhib. Conf. Power Electron., Intell. Motion*, *Renewable Energy Manage.*, 2019, pp. 1–8.

Stefan Milovanović (Student Member, IEEE) received the B.Sc. and M.Sc. degrees from the School of Electrical Engineering, University of Belgrade, Belgrade, Serbia, in 2015 and 2016, respectively, and the Ph.D. degree from the École Polytechnique Fédérale de Lausanne, Lausanne, Switzerland, in 2020.

From 2016 to 2017, he was a Research Assistant with the Department of Power Converters and Drive Systems, University of Belgrade. He is currently a Postdoctoral Researcher with the Power Electronics Laboratory, École Polytechnique Fédérale de Lausanne. His research interests include medium/high-voltage high-power conversion.

Dražen Dujić (Senior Member, IEEE) received the Dipl.-Ing. and M.Sc. degrees from the University of Novi Sad, Novi Sad, Serbia, in 2002 and 2005, respectively, and the Ph.D. degree from Liverpool John Moores University, Liverpool, U.K., in 2008, all in electrical engineering.

From 2002 to 2006, he was a Research Assistant with the Department of Electrical Engineering, University of Novi Sad. From 2006 to 2009, he was a Research Associate with Liverpool John Moores University. From 2009 to 2013, he was a Principal Scientist with ABB Corporate Research Centre, Baden, Switzerland, where he worked on the power electronics projects spanning the range from low-voltage/power switched-mode power supply in below kilowatt range to medium-voltage high-power converters in a megawatt range. From 2013 to 2014, he was an R&D Platform Manager with ABB Medium Voltage Drives, Turgi, Switzerland, where he was responsible for ABB's largest integrated-gate-commutated-thyristor-based medium-voltage drive ACS6000. He is currently an Assistant Professor with École Polytechnique Fédérale de Lausanne, Lausanne, Switzerland, where he is also the Director of the Power Electronics Laboratory. He has authored or coauthored more than 100 scientific publications and has filed 12 patents. His current research interests include design and control of advanced high-power electronics systems and high-performance drives.

Dr. Dujić received the First Prize Paper Award by the Electric Machines Committee of the IEEE Industrial Electronics Society at the 2007 Annual Conference of the IEEE Industrial Electronics Society. He received the Isao Takahashi Power Electronics Award for outstanding achievement in power electronics in 2014 and the EPE Outstanding Service Award in 2018. He is an Associate Editor for the IEEE TRANSACTIONS ON INDUSTRIAL ELECTRONICS, the IEEE TRANSACTION ON POWER ELECTRONICS, and the *IET Electric Power Applications*.